Coherent and incoherent components in near-nadir radar scattering: Applications to radar sounding of Mars

Bruce A. Campbell
Center for Earth and Planetary Studies, Smithsonian Institution, Washington, DC, USA

Michael K. Shepard
Department of Geography and Earth Science, Bloomsburg University, Bloomsburg, Pennsylvania, USA

Received 25 July 2003; revised 15 September 2003; accepted 24 October 2003; published 10 December 2003.

[1] We examine the relative importance of coherent and incoherent echo components in near-nadir radar scattering from self-affine surfaces. The coherent component, important only for observations at small incidence angles (nadir-looking sounders and altimeters), is a function of both surface roughness and scattering area. Models for the incoherent component require a minimum scattering area for validity; for smaller regions, the radar echo is overestimated. We propose a simple criterion for the horizontal scale that defines this shift in applicable scattering model and show the range of roughness parameters for which MARSIS, SHARAD, and possibly JIMO radar sounder measurements may be modeled using the two approaches. *INDEX TERMS:* 5464 Planetology: Solid Surface Planets: Remote sensing; 5494 Planetology: Solid Surface Planets: Instruments and techniques; 5470 Planetology: Solid Surface Planets: Surface materials and properties; *KEYWORDS:* radar, scattering, MARSIS, SHARAD, Mars

Citation: Campbell, B. A., and M. K. Shepard, Coherent and incoherent components in near-nadir radar scattering: Applications to radar sounding of Mars, *J. Geophys. Res.*, *108*(E12), 5132, doi:10.1029/2003JE002164, 2003.

1. Introduction

[2] Radar echoes from natural surfaces are often analyzed using theoretical models for the scattering process. In most cases, these scattering models treat the scattered field as being either "coherent" or "incoherent". The coherent component is characterized by a deterministic phase behavior (i.e., constructively interfering surface scatterers), such that the mean electric field is nonzero and the average power is given by the squared mean field. The incoherent component assumes random interference between scatterers, such that the mean electric field strength is zero, and the average power is given by the sum of the squared local field strength across the surface.

[3] In practice, there is a transitional behavior between the two components, and the total reflected power is not simply their sum. An example is to consider two point sources that radiate toward the receiving antenna. If their respective complex-valued electric fields at the receiver are given by $\mathbf{E}_1$ and $\mathbf{E}_2$, then the coherent and incoherent reflected power is

$$P_{coherent} = \mathbf{E}_1\mathbf{E}_1^* + \mathbf{E}_2\mathbf{E}_2^* + 2\mathbf{E}_1\mathbf{E}_2^* \quad (1)$$

$$P_{incoherent} = \mathbf{E}_1\mathbf{E}_1^* + \mathbf{E}_2\mathbf{E}_2^* \quad (2)$$

where the asterisk denotes the complex conjugate. For a natural surface, the received echo is the superposition of many such reflections. The difference between the two components lies in the degree of correlation between the electric field vectors. In the case of perfect correlation, the coherent component (1) contains all of the reflected power; the calculated incoherent component does not constitute additional received signal. For a diffusely scattering surface, however, the squared terms in (I) are cancelled by the random signs of the electric field cross-products, and the total reflected power is given by the incoherent component. For backscatter data collected at incidence angles typical of imaging radar systems (>20°), the incoherent echo is safely assumed to dominate the return. The coherent return is only important when the incidence angle is small (the "near-nadir" regime), since this component contributes primarily to "mirror-like" reflections from smooth portions of the surface. In this paper, we examine models for the coherent and incoherent echo components, and discuss their applicability for analysis of near-nadir radar backscatter data.

[4] Our interest in near-nadir scattering processes is motivated by two upcoming Mars radar sounder instruments. The Mars Express Mission carries the Mars Advanced Radar for Subsurface and Ionosphere Sounding (MARSIS), which operates at frequencies from 1.8 to 5 MHz. The Mars Reconnaissance Orbiter, to be launched in 2005, will carry the Shallow Subsurface Radar Sounder (SHARAD), which operates at a center frequency of 20 MHz. These sounders are intended to search for Martian subsurface geologic interfaces, but will also measure the surface return from the nadir region (and potentially from favorably oriented off-nadir regions). The surface echo may obscure subsurface returns, and significant effort is directed

0148-0227/03/2003JE002164$09.00

toward understanding the dominant scattering mechanisms and possible methods for identifying and suppressing surface reflections [e.g., *Peeples et al.*, 1978; *Orosei et al.*, 2001; *Plaut et al.*, 2001]. An additional motivation comes from the possible inclusion of a radar sounder instrument on the Jupiter Icy Moons Orbiter (JIMO) mission.

[5] This paper examines the relative importance of coherent and incoherent near-nadir radar backscattering, using a fractal description of surface roughness. Section 2 reviews the observing geometry of the MARSIS and SHARAD instruments. In section 3, we discuss existing models for these two components, and correct an error in the normalization of the coherent scattering model of *Shepard and Campbell* [1999]. We also characterize the dependence of normal-incidence backscatter on surface roughness and scattering area. Section 4 assesses the range of validity for models of incoherent scattering, and the conditions under which coherent surface returns may be observed, relative to the operating parameters of the MARSIS and SHARAD sounders.

2. MARSIS and SHARAD Observations

[6] MARSIS and SHARAD use synthetic-aperture Doppler processing techniques to achieve improved spatial resolution in the along-track direction. Combined with the delay resolution achieved with a chirped (wide-bandwidth) pulse, the sounder data may be processed to form a delay-Doppler array of "resolution cells" centered on the nadir point (Figure 1). Because the antenna beam is directed toward the nadir, the delay-Doppler array is ambiguous to the left and right of the ground track. Possible subsurface echoes will appear in the array "bin" appropriate to their round-trip delay and frequency shift. For this paper, we ignore the subsurface reflections and examine the possible range of behavior in the surface echoes.

[7] The term "clutter" is used in radar sounding to refer to off-nadir surface echoes that can be confused with true subsurface reflections (since both arrive at greater delay than the nadir surface point). We extend this definition here to include the nature of the surface return from the nadir region. Clutter may have "random" and "deterministic" components. The random component can be considered to represent surface roughness on scales much smaller than the resolution cells (e.g., small hills, boulder fields, dunes), such that its average behavior is well represented by an angular backscatter function. The deterministic component arises from tilted, discrete off-nadir features (e.g., large hillsides, crater walls) or from locally smooth patches in the nadir region. In general, random clutter may be treated with models for the incoherent radar scattering component. Deterministic off-nadir clutter, and the nadir return, may have a strong coherent component under conditions discussed below.

3. Radar Scattering Models

[8] In this work, we deal with surfaces described by self-affine, or fractal, statistics. For a fractal surface, roughness may be described by the RMS slope (the ratio of the Allan deviation to the horizontal step size) at some reference scale and the Hurst exponent, H [e.g., *Shepard et al.*, 2001]. We use the illuminating wavelength, λ, as the reference horizontal scale, and denote the corresponding RMS slope as s_λ. The RMS slope at any other scale, x, is given by

$$s_x = s_\lambda \left(\frac{x}{\lambda}\right)^{H-1} \tag{3}$$

Higher values of H correspond to surfaces whose RMS slope declines more slowly with x than that of low-H surfaces. Fractal surface profiles are also described by a power law form of the surface height power-spectral density function, $S(f)$:

$$S(f) = S_o \left(\frac{f}{f_o}\right)^{-2H-1} \tag{4}$$

where S_o is a scaling factor (m^3), f is the spatial frequency, and f_o is a reference frequency [*Turcotte*, 1992].

3.1. Scattering Model for the Coherent Component

[9] In general, coherent radar echoes are confined to situations where the reflecting region is very smooth at the scale of the illuminating wavelength, λ, and is oriented nearly perpendicular to the incident beam. Because the coherent return requires constructive interference between surface scattering elements, this mechanism is also limited to scattering areas (i.e., resolution cells) whose total RMS height deviation is much less than λ. In effect, we treat the scattering region as an antenna (or single "facet") whose coherent gain is reduced by surface roughness. This is the basis for the reduction in effective surface reflectivity with RMS height discussed by *Barrick and Peake* [1967]. Our contribution in this paper is to treat the coherent scattered component from a self-affine surface of finite extent.

[10] The coherent scattered electric field from a rough fractal surface was initially derived by *Shepard and Campbell* [1999], exploiting the fact that surface heights along concentric annuli about any chosen point have an RMS value (with respect to the mean plane surface), ξ, that is related to the radius of the annulus, r, the RMS slope at the wavelength scale, and the Hurst exponent:

$$\xi(r) = \frac{\lambda}{\sqrt{2}} s_\lambda \left(\frac{r}{\lambda}\right)^H \tag{5}$$

The coherent backscattered field for each annulus is reduced, relative to that of a smooth plate, by the factor

$$\exp\left[-2k^2 \xi(r)^2 \cos^2 \phi\right] \tag{6}$$

where $k = 2\pi/\lambda$ and ϕ is the radar incidence angle. The total scattered field is the integral over all annuli within a given uniformly illuminated area:

$$E_s = E_o\left[ie^{-ikZ}\right] \frac{2\pi\lambda R_e}{Z} \int_o^{\hat{r}_{\max}} \exp\left[-4\pi^2 s_\lambda^2 \hat{r}^{2H} \cos^2 \phi\right] \hat{r} \cdot J_o(4\pi \hat{r} \sin \phi) d\hat{r} \tag{7}$$

where Z is the vertical distance from the observer to the center of the target area, E_o is the illuminating field, J_0 is a Bessel function of the first order, R_e is an effective

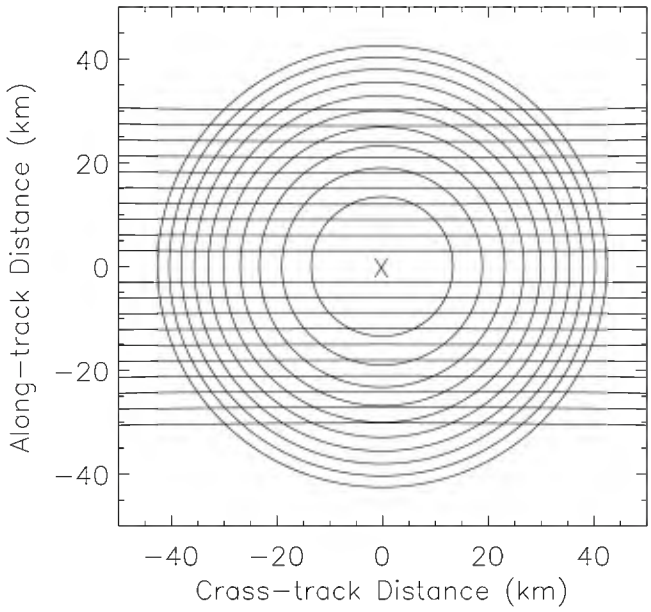

Figure 1. Schematic of range and Doppler frequency "bins" for a radar sounder. The spacecraft nadir point is shown by the "X", and the flight direction is along the vertical axis. Lines of constant time delay form rings about the subradar point, while iso-frequency contours form hyperbolic curves. Note that the spatial scale of the resolved elements changes over the surface footprint. For MARSIS and SHARAD, it is not possible to discriminate whether echoes in a given delay and Doppler bin arise from the left or right side of the flight line.

reflectivity, and we introduce the dimensionless variable $\hat{r} = r/\lambda$. $\hat{r}_{\max}$ is thus the radius of the scattering area in multiples of λ (Figure 2). The dimensionless backscatter coefficient, σ^o, is defined by

$$\sigma^o = \frac{4\pi Z^2 \mathrm{Re}\left(|E_s|^2\right)}{A_o \mathrm{Re}\left(|E_o|^2\right)} \tag{8}$$

where A_o is the scattering area [*Ulaby et al.*, 1982]. Note that the definition of the backscatter coefficient is identical for coherent and incoherent echoes; only the scattered field changes, depending upon our surface scattering model. If we let the integral in (7) be given by K, the backscatter coefficient of the coherent component for the fractal surface is:

$$\sigma^o_{coherent} = \frac{16\pi^2 R_e^2 K^2}{\hat{r}^2_{\max}} \tag{9}$$

Note that, in the limit of a flat plate, R_e^2 is identical to the Fresnel normal reflection coefficient, ρ_o. This expression represents a correction to equations (22)–(24) of *Shepard and Campbell* [1999], which did not properly normalize for the scattering area.

[11] We may obtain some physical insight from the behavior of a mirror-like smooth surface, which will exhibit the maximum possible normal-incidence backscatter coefficient for any given reflectivity. A finite smooth disc is characterized by $s_\lambda = 0$, yielding

$$\sigma^o_{coherent}(s_\lambda = 0) = R_e^2 \left[\frac{J_1(4\pi \hat{r}_{\max} \sin\phi)}{\sin\phi}\right]^2 \tag{10}$$

When $\phi = 0$:

$$\sigma^o_{coherent}(\phi = 0, s_\lambda = 0) = 4\pi^2 R_e^2 \hat{r}^2_{\max} \tag{11}$$

This result is in agreement with the derivation cited by *Ulaby et al.* [1982, equation [10.22]] for the behavior of a flat, conducting circular plate, which has a normal-incidence radar cross section (m^2) of $4\pi A_o^2/\lambda^2$. The backscatter coefficient is thus $4\pi A_o/\lambda^2$. Substituting $A_o = \pi r^2_{\max}$, $\hat{r}_{\max} =$

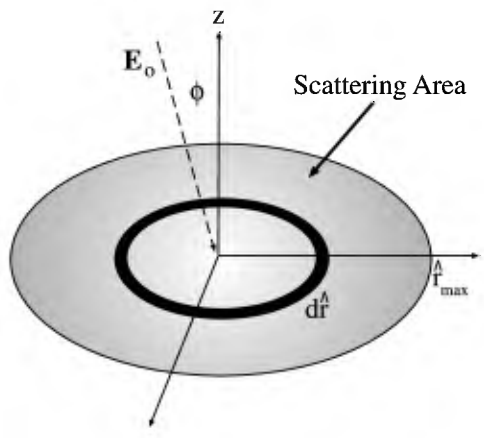

Figure 2. Diagram of scattering geometry and descriptive parameters used in the coherent scattering model. The gray region denotes a particular sounder "resolution cell", where $\hat{r}_{\max}$ is the dimensionless radius (radius/illuminating wavelength). The incident field, $\mathbf{E}_o$, encounters the surface at an incidence angle, ϕ. The black ring shows one contributing annulus of the coherent field integration in (7).

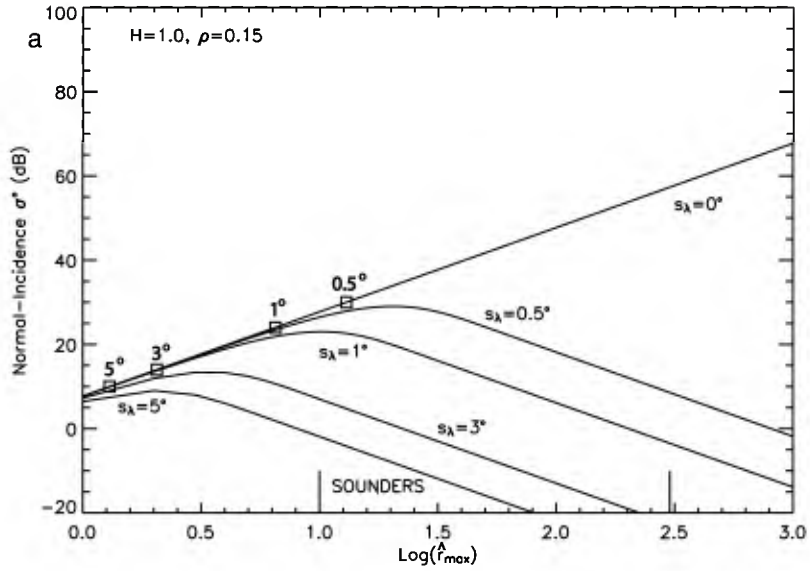
a
H=1.0, ρ=0.15
Normal-Incidence σ° (dB)
Log(r̂max)
sλ=0°
sλ=0.5°
sλ=1°
sλ=3°
sλ=5°
0.5°
1°
3°
5°
SOUNDERS

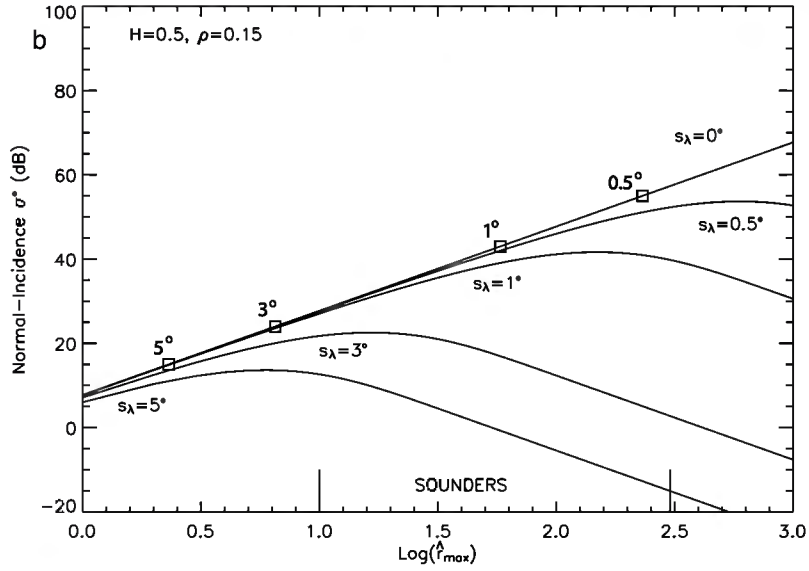
b
H=0.5, ρ=0.15
Normal-Incidence σ° (dB)
Log(r̂max)
sλ=0°
sλ=0.5°
sλ=1°
sλ=3°
sλ=5°
0.5°
1°
3°
5°
SOUNDERS

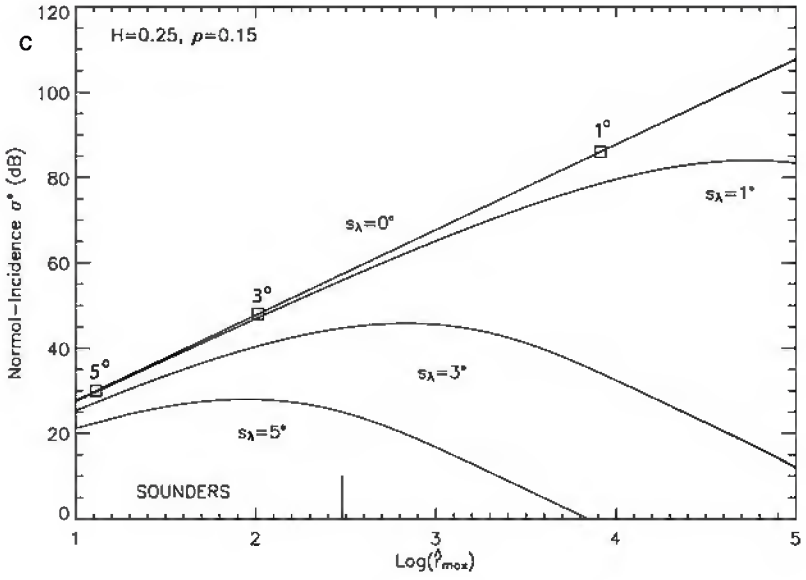
c
H=0.25, ρ=0.15
Normal-Incidence σ° (dB)
Log(r̂max)
sλ=0°
sλ=1°
sλ=3°
sλ=5°
1°
3°
5°
SOUNDERS

r_{max}/λ, and adding the effective reflectivity of a dielectric plate, we obtain (11). Note that a fully illuminated smooth spherical scatterer with radius $\gg\lambda$ has a backscatter coefficient independent of its radius ($\sigma^o = \rho_o$), since the coherently scattering region at the front cap expands at the same rate as the total projected area of the sphere [*Bohren and Huffman*, 1983].

[12] For a mirror-like surface, the normal-incidence backscatter coefficient for the coherent echo increases with the scattering area. On a rough surface ($s_\lambda > 0$), σ^o is reduced from the maximum value given by (10), similar to the exponential decline in coherent reflectivity noted by *Barrick and Peake* [1967]. As the scattering area increases, even surfaces with very low s_λ will eventually exhibit a negligible coherent backscatter coefficient. The reason lies in the nature of the coherent summation and the power law increase in RMS height with distance from any given point (5). For any choice of s_λ and H, there is a value of $\hat{r}_{max}$ beyond which the local coherent contributions begin to destructively interfere. The analogy is to consider the area around a given point as an antenna of some surface tolerance. While we may achieve strong backscatter gains from any one such aperture, a group of antennas with arbitrary phase would have no net coherent component. This arbitrary phase is introduced as the RMS height of annuli about some center point exceeds a fraction of the wavelength.

3.2. Scattering Models for the Incoherent Component

[13] The incoherent component of radar scattering may be treated with a variety of methods, including the small-perturbation, integral equation, and Kirchhoff models [e.g., *Barrick and Peake*, 1967; *Ulaby et al.*, 1982; *Hagfors*, 1964; *Fung et al.*, 1992; *Franceschetti et al.*, 1999]. The latter approach requires that the surface be smooth ("quasi-specular") on horizontal scales comparable to the illuminating wavelength. For backscatter, the reflected power is the incoherent sum of echoes from surface patches oriented perpendicular to the incident beam, which in the high-frequency limit is represented by the slope distribution along a profile line [*Muhleman*, 1964; *Simpson and Tyler*, 1982].

[14] In the widely used *Hagfors* [1964] model, the surface is described by the root-mean square of the surface tilt distribution, θ_{rms}, and the Fresnel normal reflectivity ρ_o. Hagfors assumed an exponential form for the surface height autocorrelation function, approximating its derivative near the origin, to obtain

$$\sigma^o_H(\phi) = \frac{C\rho_o}{2}\left[\cos^4\phi + C\sin^2\phi\right]^{-3/2} \tag{12}$$

where C is taken to be $1/\tan^2(\theta_{rms})$. The specific horizontal scale linked with θ_{rms} is not defined, and in some instances the surface is taken to have a scale-invariant RMS slope (i.e., $H = 1$ in (3)) for all length scales greater than a few times the incident wavelength. At normal incidence,

$$\sigma^o_H(0) = \frac{C\rho_o}{2} \tag{13}$$

The incoherent backscatter coefficient for a self-affine surface is derived by *Franceschetti et al.* [1999] and *Biccari et al.* [2001]. We cite the latter model here:

$$\sigma^o_B(\phi) = \frac{\rho_o}{H\cos^2\phi}\left[\frac{(2\pi)^{(H-1)}}{s_\lambda\sqrt{2}\cos\phi}\right]^{2/H} \cdot\sum_{n=0}^{\infty}(-1)^n\frac{\sin^{2n}\phi}{(n!)^2}\left[\frac{(2\pi)^{(H-1)}}{s_\lambda\sqrt{2}\cos\phi}\right]^{2n/H}\Gamma\left(\frac{n+1}{H}\right) \tag{14}$$

At normal incidence, only the zeroth-order term of the summation in (14) is nonzero.

For H = 0.25,

$$\sigma_B(0) = \frac{3\rho_o}{128\pi^6 s_\lambda^8} \tag{15}$$

for $H = 0.5$,

$$\sigma_B(0) = \frac{\rho_o}{8\pi^2 s_\lambda^4} \tag{16}$$

and for $H = 1.0$,

$$\sigma^o_B(0) = \frac{\rho_o}{2s_\lambda^2} \tag{17}$$

[15] The normal-incidence incoherent backscatter coefficient for a self-affine surface is thus analogous to the Hagfors model when $H = 1$, if we assume that $C = s_\lambda^{-2}$. In contrast, the angular scattering law derived from (14) is generally similar to the Hagfors solution when $H = 0.5$. These properties may be attributable to the nonfractal nature of a surface with an exponential autocorrelation function. The power spectrum of such a surface is

$$S(f) = \frac{S_o}{\pi + 4\pi^3 f^2 L_c^2} \tag{18}$$

where L_c is the correlation length [*Li et al.*, 2002]. For high frequencies, this approaches an $H = 0.5$ behavior, which may explain the correlation in scatter-law shape between the Hagfors and fractal models. The normal-incidence behavior given by (17) is typical of geometric optics models, perhaps independent of the functional form of the surface slope distribution at other angles.

3.3. Backscatter as a Function of Illuminated Area and Roughness

[16] Both the coherent and incoherent scattering mechanisms have a relationship to the scale of the scattering area.

Figure 3. (opposite) Normal incidence backscatter coefficient versus $\log(\hat{r}_{max})$ as a function of wavelength scale RMS slope, s_λ, for three values of the Hurst exponent: (a) $H = 1.0$, (b) $H = 0.5$, (c) $H = 0.25$. The solid straight line in each graph is the behavior of a mirror-like surface. The square symbols represent the minimum $\hat{r}_{max}$ values consistent with the incoherent scattering model at each value of s_λ. Note that the incoherent model may be considered "valid" for $\hat{r}_{max}$ values to the right of each square. Curved solid lines show the coherent scattering coefficient for the corresponding RMS slope. The possible range of values for MARSIS and SHARAD observations (~10 to ~300) is noted at bottom.

For the coherent return, the dependence on scale is represented by the dimensionless $\hat{r}_{max}$ term in (9). As we will show below, the maximum coherent backscatter coefficient, for some H and s_λ, occurs over a narrow range of $\hat{r}_{max}$ values. Models for the incoherent component, such as (14), are predicated on the assumption that the surface is statistically well sampled, such that the predicted σ^o value is invariant with scattering area. In previous studies of scattering from gently undulating surfaces, this constraint is expressed as $L \gg L_c$, where L is the lateral dimension of the scattering region [*Ulaby et al.*, 1982].

[17] As H or s_λ declines, a self-affine surface becomes more smooth with respect to a given radar wavelength, eventually approaching a mirror-like behavior. The assumptions underpinning (14) break down when the scattering region does not adequately sample the surface slope distribution (i.e., "facet" population). For any given values of H and s_λ, (14) yields a value for $\sigma^o(0)$, but for a very smooth surface this predicted backscatter coefficient may exceed that of a planar target of equal area (11). Since the planar target sets a maximum limit on the backscatter from a natural surface, we may set a lower limit on $\hat{r}_{max}$ to avoid physically unrealistic situations:

$$\hat{r}_{max} > \left[\frac{\sigma_B^o(\phi = 0, H, s_\lambda)}{4\pi^2 \rho_o}\right]^{1/2} \tag{19}$$

[18] To illustrate these behaviors, we compare the backscatter coefficients of the coherent (9) and incoherent (14) components, at normal incidence, as a function of scattering area and roughness. For each pair of H and s_λ values, we determine $\sigma_B^o(0)$ from (14), and a minimum scattering area from (19). We then calculate the coherent echo as a function of $\hat{r}_{max}$, using a numerical integration of (7). These results are shown in Figure 3, where we have assumed that $R_e^2 \sim \rho_o$, and set both equal to 0.15. The squares in each plot represent the incoherent backscatter coefficients, plotted at their corresponding minimum $\hat{r}_{max}$ values. The curved lines are the backscatter coefficients of the coherent echo for each value of s_λ.

[19] Interestingly, the minimum $\hat{r}_{max}$ values from (19) are just below the scale at which the coherent echo is a maximum for any chosen roughness parameters. The coherent component declines relatively quickly for other values of $\hat{r}_{max}$. The minimum scattering area required for validity of (14) increases for lower values of H and s_λ; smoother surfaces therefore require a larger surface resolution cell. For $H \geq 0.5$, and reasonable values of s_λ, the required horizontal dimension of the scattering area is typically $<10^3\lambda$, but for lower Hurst exponents and low RMS slope the necessary scale can exceed $10^6\lambda$. If a given radar observation yields a resolution cell whose maximum horizontal radius is less than that given by (19) for the particular roughness (H and s_λ), the coherent model provides a more realistic estimate of the backscattered power.

4. Implications for MARSIS and SHARAD Observations of Mars

[20] The MARSIS and SHARAD radar sounders employ low-frequency (1.8–20 MHz) signals to penetrate the upper crust of Mars and reveal buried geologic interfaces. From the discussion above, we suggest that surface coherent returns will be strongly dependent upon the size of resolved surface elements with respect to the radar wavelength. The maximum horizontal extent of these resolved surface elements varies considerably over the illuminated area (Figure 1). For SHARAD, the free-space range resolution, Δr, is 30 m (10 MHz bandwidth), while for MARSIS Δr = 300 m (1 MHz bandwidth). Doppler processing of the radar echoes yields along-track spatial resolution, Δa, of 0.3–1.0 km for SHARAD and 5–9 km for MARSIS.

[21] The first sounder range "bin" contains echoes from a region of radius

$$r_o = \sqrt{h^2 + (h + \Delta r)^2} \tag{20}$$

where h is the spacecraft altitude. Both Mars sounders operate at minimum altitudes near 300 km, for which r_o = 4.2 km for SHARAD and 13.4 km for MARSIS. The corresponding $\hat{r}_{max}$ values (ratio of resolution cell radius to radar wavelength) are 280 for SHARAD and 80–220 over the range of MARSIS wavelengths. Each succeeding range bin narrows, until at some point the projected cross-track spatial resolution becomes smaller than Δa.

[22] For example, the tenth range bin for SHARAD, corresponding to an incidence angle of 2.6°, has Δr = 0.7 km. The $\hat{r}_{max}$ value is related to one-half the maximum dimension of the scattering area (Figure 2), so in this case $\hat{r}_{max} \sim 23$. For areas further from the subradar point, the azimuth resolution will eventually set a minimum limit on $\hat{r}_{max}$, with values of ~10–30 (Δa = 0.3–1.0km). For MARSIS, the along-track resolution determines $\hat{r}_{max}$ for all but the first range bin, with values of 80–150 for the 60-m wavelength, and 30–54 for λ = 167 m. In contrast, the Magellan altimeter system resolved cells with $\hat{r}_{max} > 8{,}000$; at these scales coherent echoes are likely negligible [*Ford and Pettengill*, 1992].

[23] Values of the Hurst exponent and wavelength-scale slope for Mars at scales of 15–170 m must, at present, be inferred from analysis of MOLA data with ~300 m horizontal sampling. On the basis of these data, the Martian surface is characterized by an average H value of 0.7–0.8, with values of $H < 0.5$ confined primarily to the midlatitude northern plains [*Orosei et al.*, 2003]. The issue of whether the power law behavior of surface roughness extends to smaller scales (e.g., 15 m for SHARAD) remains open to debate, but these values are very likely reasonable within the wavelength range of the MARSIS sounder [*Campbell et al.*, 2003].

[24] Because the sounder observations may encompass surface resolution elements with relatively small $\hat{r}_{max}$ values (10–300), the validity of (14) for incoherent returns, and the contribution of coherent scattering, may vary dramatically with roughness and viewing geometry (i.e., the position of a reflecting surface area in delay-Doppler space). For this range of $\hat{r}_{max}$, and the data shown in Figure 3, we may define some broad guidelines for the SHARAD and MARSIS observations:

[25] (1) $H \sim 1$: the incoherent scattering model is valid for $s_\lambda > 0.5°$, and coherent echoes may be significant if $s_\lambda < 1°$.

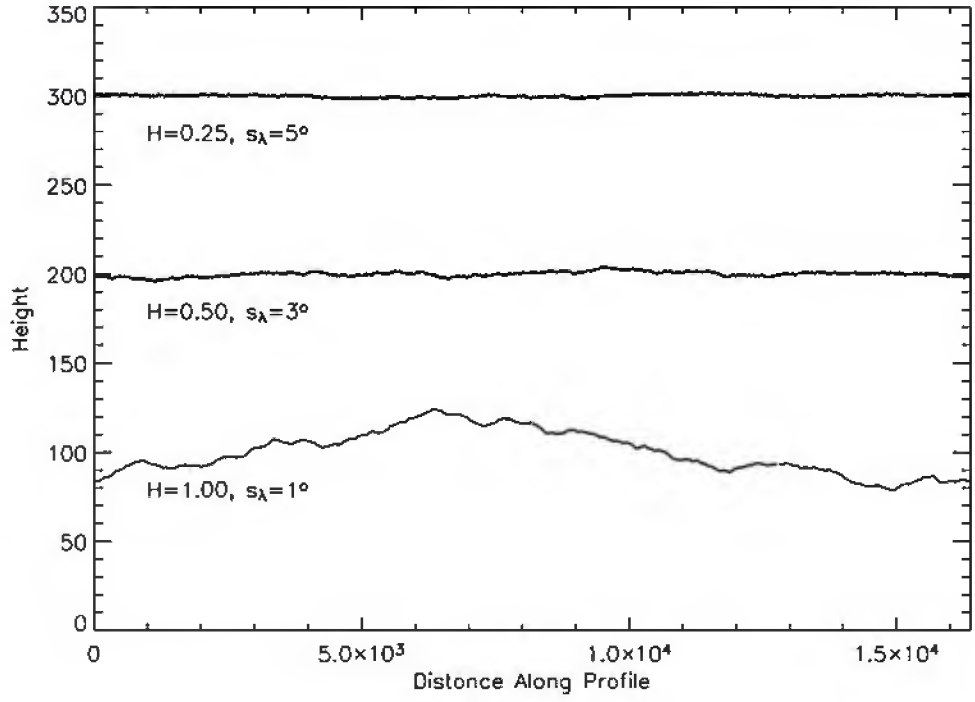

Figure 4. Synthetic fractal profiles that illustrate the upper limit on roughness at the wavelength scale, s_λ, for significant coherent backscattered returns in MARSIS or SHARAD data as a function of the Hurst exponent, H. The illuminating wavelength in these plots is one unit along the horizontal axis. The plots are offset vertically for clarity. Note that surfaces with higher values of H have more rolling terrain, and must be "smoother" at a given reference scale in order to permit effective coherent scattering.

[26] (2) $H \sim 0.5$: the incoherent model is valid for $s_\lambda > 2°$, and coherent echoes may be significant if $s_\lambda < 3°$.

[27] (3) $H = 0.25$: the incoherent model is valid for $s_\lambda > 4°$, and coherent returns may be significant if $s_\lambda < 5°$.

[28] Synthetic fractal profiles that correspond to these upper limits on roughness for the coherent scattering model are shown in Figure 4. Note that higher values of H lead to more rapid increases in roughness with horizontal scale, so the roughness at the wavelength scale must be commensurately lower to permit significant coherent returns for a specific range of $\hat{r}_{max}$ values. Because surfaces with lower values of H have stronger coherent echoes for any value of s_λ, we expect that such behavior will be most often observed in the smooth northern plains of Mars.

5. Conclusions

[29] We have examined the relative importance of coherent and incoherent echo components in near-nadir scattering from self-affine surfaces. These results agree with previous models that show the coherent backscatter coefficient is a function of both surface roughness and scattering area. Models for the incoherent echo from fractal surfaces are limited in their application to scattering areas large enough to sample the surface slope distribution. For smaller scattering areas, a coherent model for scattering from a slightly rough region is more realistic. The MARSIS and SHARAD sounders resolve surface areas on the order of 10–300 wavelengths in scale, in contrast to radar altimeters such as Magellan that have resolution cells of >8,000 λ. As a result, coherent echoes may be present in sounder returns when wavelength-scale RMS slope values are less than 1°–5°, with lower cutoff values for increasing H. Very smooth surfaces, though limited in occurrence on Mars, may thus exhibit near-nadir scattering behavior that varies as a function of the horizontal dimensions of delay-Doppler resolution elements.

[30] **Acknowledgments.** The authors thank P. Ford, T. Hagfors, R. Phillips, and R. Simpson for helpful discussions and comments on the manuscript. The comments of two reviewers are also appreciated. This work was supported in part by grants from NASA's Planetary Geology and Geophysics Program (BAC and MKS) and the NASA Mars Reconnaissance Orbiter project (BAC).

References

Barrick, D. E., and W. H. Peake, Scattering from surfaces with different roughness scales: Analysis and interpretation, *Electrosci. Lab. Rep. 1388-26*, Ohio State Univ., Columbus, 1967.

Biccari, D., G. Picardi, R. Seu, and P. T. Melacci, Mars surface models and subsurface detection performance in MARSIS, paper presented at International Geoscience and Remote Sensing Symposium, Inst. of Electr. and Electron. Eng., Sydney, Australia, 2001.

Bohren, C. F., and D. R. Huffman, *Scattering and Emission From Small Particles*, John Wiley, New York, 1983.

Campbell, B. A., R. R. Ghent, and M. Shepard, Limits on inference of Mars small-scale topography from MOLA data, *Geophys. Res. Lett.*, *30*(3), 1115, doi:10.1029/2002GL016550, 2003.

Ford, P. G., and G. H. Pettengill, Venus topography and kilometer-scale slopes, *J. Geophys. Res.*, *97*, 13,102–13,114, 1992.

Franceschetti, G., A. Iodice, M. Migliaccio, and D. Riccio, Scattering from natural rough surfaces modeled by fractional Brownian motion two-dimensional processes, *IEEE Trans. Antennas Propag.*, *47*, 1405–1415, 1999.

Fung, A. K., Z. Li, and K. S. Chen, Backscattering from a randomly rough dielectric surface, *IEEE Trans. Geosci. Remote Sens.*, *30*, 356–369, 1992.

Hagfors, T., Backscattering from an undulating surface with applications to radar returns from the Moon, *J. Geophys. Res.*, *69*, 3779–3784, 1964.

Li, Q., J. Shi, and K. S. Chen, A generalized power law spectrum and its applications to the backscattering of soil surfaces based on the integral equation model, *IEEE Trans. Geosci. Remote Sens.*, *40*, 271–280, 2002.

Muhleman, D. O., Radar scattering from Venus and the Moon, *Astron. J.*, *69*, 34–41, 1964.

Orosei, R., R. Bianchi, A. Coradini, S. Espinasse, C. Federico, and A. Ferriccioni, Characterization of the Martian surface scattering at decametric wavelengths (abstract), in *Conference on the Geophysical Detection of Subsurface Water on Mars*, *LPI Contrib. 1095*, Lunar and Planet. Sci., Houston, Tex., 2001.

Orosei, R., R. Bianchi, A. Coradini, S. Espinasse, C. Federico, A. Ferriccioni, and A. I. Gavrishin, Self-affine behavior of Martian topography at kilometer scale from Mars Orbiter Laser Altimeter data, *J. Geophys. Res.*, *108*(E4), 8023, doi:10.1029/2002JE001883, 2003.

Peeples, W. J., et al., Orbital radar evidence for lunar subsurface layering in Maria Serenitatis and Crisium, *J. Geophys. Res.*, *83*, 3459–3468, 1978.

Plaut, J. J., R. Jordan, A. Safaeinili, G. Picardi, R. Seu, and R. Orosei, Subsurface sounding of Mars: The effects of surface roughness (abstract), *Conference on the Geophysical Detection of Subsurface Water on Mars*, *LPI Contrib. 1095*, Lunar and Planet. Sci., Houston, Tex., 2001.

Shepard, M. K., and B. A. Campbell, Radar scattering from a self-affine fractal surface: The near-nadir regime, *Icarus*, *141*, 156–171, 1999.

Shepard, M. K., B. A. Campbell, M. Bulmer, T. Farr, L. R. Gaddis, and J. Plaut, The roughness of natural terrain: A planetary and remote sensing perspective, *J. Geophys. Res.*, *106*, 32,777–32,795, 2001.

Simpson, R. A., and G. L. Tyler, Radar scattering laws for the lunar surface, *IEEE Trans. Antennas Propag.*, *AP-30*, 438–449, 1982.

Turcotte, D. L., *Fractals and Chaos in Geology and Geophysics*, Cambridge Univ. Press, New York, 1992.

Ulaby, F. T., R. K. Moore, and A. K. Fung, *Microwave Remote Sensing*, Addison-Wesley-Longman, Reading, Mass., 1982.

B. A. Campbell, Center for Earth and Planetary Studies, Smithsonian Institution, Washington, DC 20560-0315, USA. (campbellb@nasm.si.edu)

M. K. Shepard, Department of Geography and Earth Science, Bloomsburg University, 116B Hartline Center, Bloomsburg, PA 17815, USA.